THESIS

MSc by Research

Nano-Resists for Next Generation Semiconductors

By

Filip Robert Krzymieniecki ([redacted])

29th of August 2023

Abstract

The incorporation of nanoparticles can improve material characteristics, with their small particle size providing distinctive benefits. Nanocomposite resists in the semiconductor industry can improve feature resolutions on the nanometre scale or etch resistance, with applications including more energy efficient MEMS and novel sensors.

This thesis focuses on integrating nickel nanoparticles into photoresists to improve the etch resistance of the material. Increased etch resistance enables the production of deep trenches with nano feature sizes, as well as maintaining samples with even geometry of the structures.

The experiments were set up to test the etch resistance of samples with different loading of nickel nanoparticles. Commercially purchased nanoparticles were used for the experiments, as a basis for future use of the nanoparticles produced by MACS (Matrix Assembly Cluster Source) tool. The etch tests were conducted in SPTS systems, an APS (advanced plasma source) tool designed for etching of strongly bonded materials and a DSi-v tool designed for etching Si for vertical sidewalls with the Bosch process. Ellipsometry was used to obtain the differences in thickness pre- and post-etching of the samples, data which was used to calculate the sample etch rates. SEM imaging was used to study the texture of the nanocomposite resists. For the commercially purchased nanoparticle samples, MIR-701 photoresist was used.

The results show a positive relationship between the nickel loading and the etch resistance, with an increase of as much as 17% over the control sample. At the structural level, the nanoparticles were integrated into the photoresist successfully, with an even film surface.

Declaration

This work has not previously been accepted in substance for any degree and is not being concurrently submitted in candidature for any degree.

Signed: 

Date: 29/08/2023

This thesis is the result of my own investigations, except where otherwise stated. Other sources are acknowledged by footnotes giving explicit references. A bibliography is appended.

Signed: 

Date: 29/08/2023

I hereby give my consent for my work, if relevant and accepted, to be available for photocopying and for inter-library loans **after expiry of a bar on access approved by the University.**

Signed: 

Date: 29/08/2023

The University's ethical procedures have been followed and, where appropriate, that ethical approval has been granted.

Signed: 

Date: 29/08/2023

Table of Contents

List of Figures

Acknowledgements

In this section I would like to express my deepest gratitude to all of the people that had aided me during my project. In their own individual ways, they have helped me to navigate the complex processes involved and gave me invaluable training without which I would not be able to deliver this thesis.

First, I would like to thank Prof. Richard Palmer for giving me the opportunity to work on this project and providing valuable corrections of this thesis. His support throughout helped me to investigate new directions and methods to achieve my goals and complete the project in the shadow of the coronavirus. This project had set me on a new course in life that I experience every day and opened new and bright horizons in my personal and professional life.

Dr Jacob Mitchell and Dr Jon Evans provided me with indispensable support throughout this project, helping me every day in the lab in order to understand lithography and etch processes and providing me with advice and corrections for this thesis. I would like to thank them both, as well as everyone else in the lab, for their patience with me as a student and providing me with a pleasant work environment in the cleanroom.

Dr Huma Ashraf was a very valuable industrial supervisor based in the SPTS/KLA office in Newport. In addition, I thank the SPTS engineers Chris and Kerry for providing me with etch advice in their spare time.

Special thanks to the Swansea NanoLab group, with who I was able to discuss my work and who provided me with support throughout, especially Sean Lethbridge for helping me with TEM support.

I could not have completed this project without the support of my friends and family, who have helped me to stay on track throughout.

1.0 Introduction

1.1 Research Background and Motivation

It is predicted that nano-composite resist materials will play a key role in the continuing miniaturisation of semiconductors (Moore's Law) through photo-, EUV- and ebeam-lithography, for example by helping to increase the feature resolution [1]. Nano-fillers can be carbon-based, metal or metal oxides. Crucially, new nanofillers have the potential to accelerate the application of new semiconductor materials such as GaN and SiC. These high band gap, hard materials with applications in e.g., power electronics need high etch-resistance resists to achieve deep, high-resolution etching [1]. The exciting possibilities for the advancement of these materials through the addition of nanoparticles, mean that this research has exciting potential.

1.2 Aims and Objectives

The main objective of this research is to develop and test a nanocomposite resist, with the aim to improve the etch resistance obtained in plasma etch tools. The resist must be easily integrable into production lines to exploit the impact of the research. The etch rate should be manifest over a wide range of loadings of the nanoparticles; if the effects are only detectable at very high loadings, it will reduce the cost effectiveness of the resist materials. The new resist will be compared against SiO_2 as an etch mask, since in the fab production process this is seen as harder compared with resist materials, which are in fact used more often to pattern an SiO_2 hardmask layer rather than the silicon itself. If the nanocomposite resist will be comparable to SiO_2, that would be a big improvement.

1.3 Environmental Impact of the Research

The impregnation of nanomaterials can add new functions and increase the production efficiency of semiconductor materials. Nanoparticles display promising properties, especially when the amount of the material is considered, as the specific surface area increases the smaller the particles are. This means that the impregnation of nanomaterials can significantly improve the production process potential at a proportionately low material cost. Also, as the fabrication processes for microchips improve, allowing higher resolution and thus higher density of transistors in the final product, it will enable a further decrease in chip size without compromising power delivery thus creating a material saving. As the demand for innovative semiconductor

technology rises, such innovations will drive the delivery of more energy efficient transistors, building blocks which are at the forefront of new technology and clean energy transition.

On the other hand, the research itself is likely to generate some unenviable chemical waste produced through mistakes or excess use. The laboratories also consume more energy on average than the rest of the university. For this reason, as well as safety, it is important to ensure that the most sustainable research options are considered in terms of planning and ordering materials for experiments. Moreover, ordering will only be done through companies that can ensure that their materials are responsibly sourced.

2.0 Literature Review

2.1 Introduction to Photoresists

Photoresists play a key role in the manufacture of semiconductors, fundamental components for the production of microelectronic equipment and devices across a wide range of industries. There exists a wide array of photoresist materials (PR), which could be divided into negative and positive tone. The specific chemistry of the photoresist allows it to be developed using different chemicals after patterning. Etch resistance of a photoresist is a key factor, especially for hard materials such as Silicon Carbide. This process is a major issue in the process of manufacturing semiconductors, and a key concern for the sponsor company SPTS/KLA.

An interesting approach is the impregnation of nanofillers into the PR, which can give the material unique properties. The nanomaterials can range from metallic, magnetic, carbon-based, to luminescent materials [2]. However, this study will focus only on inorganic metal clusters. This section will go into detail about the benefits of adding of nanoparticles within photoresist, how they can affect the material properties and give additional functionality for example in sensor production. Different techniques of integrating the nanoparticles, as well as background information about some of the main materials involved, will be discussed.

2.2 Lithography Processes

Lithography (from the Greek, “lithos” meaning stone and “grafia” meaning to write) is a process of patterning a film of photoresist at micro or nanometre scales [3]. In the process, the substrate (e.g., Si, SiC) is covered with a photoresist layer (e.g., HMDS, PMMA), using a variety of methods such as spin coating, spray coating or dip coating. A bake step following application of the resist onto the substrate allows for evaporation of the solvent (e.g., Anisole, ethyl-lactate), leaving the photoresist on the substrate. A pattern is projected onto the photoresist by the use of radiation, the type of which is dependent on the resist used (e.g., E-Beam, UV). The radiation reacts with the exposed areas causing either scission or cross linking for most polymer resists, depending on whether the resist is positive tone or negative tone. Development will cause the removal of either the exposed or unexposed areas, respectively. Then, the process can be described as a series of steps. The final structure is set the resist used and process conditions. A diagram of the process steps is shown on Figure 1 below.

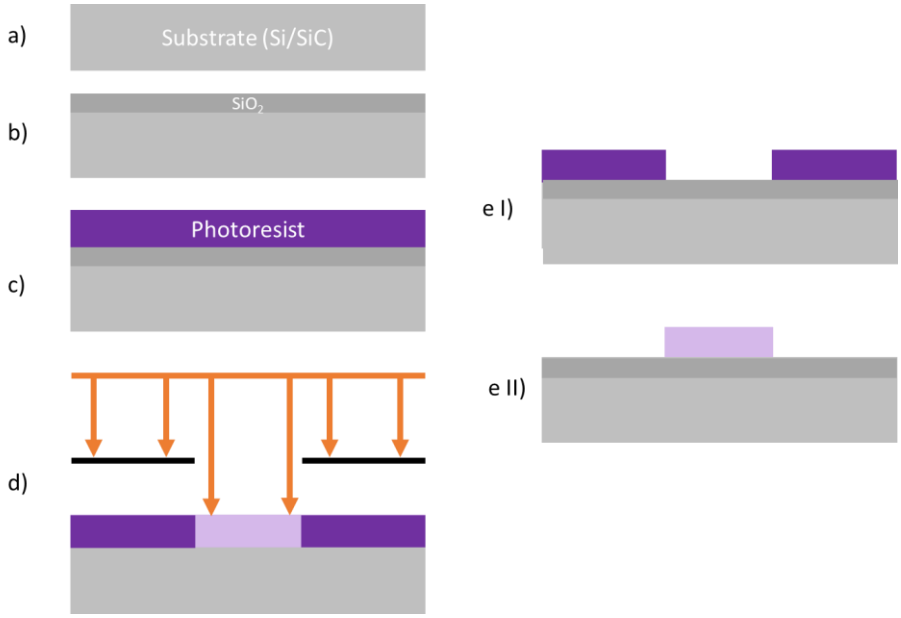

Figure 1: Step by step example of a basic lithography process showing a) the base substrate wafer; b) an oxide hard mask layer deposited on top of the substrate; c) depositing of the photoresist by spin coating, followed by the soft baking process; d) exposure of parts of the resist to radiation; e) development of the resist in the cases of I) negative and II) positive tone resists.

2.2.1 Substrate Materials

The substrate, or the wafer, is the material on which the integrated circuits are fabricated, and typically represents the semiconductor material to be processed into functional architectures. This section will describe some of features of important substrate materials.

2.2.1.1 Silicon

Silicon single crystals are the standard base material for microsystems technology or micro-electrical mechanical systems. One of the reasons behind the success of silicon is the mechanical strength of the material, which is derived from its atomic crystalline structure; it ensures that it is almost a perfect Hookean material (displays elastic behaviour, where shear strain is proportional to the resulting stress), and the energy dissipation is limited due to its structure. Additionally, silicon is readily available from silica in the environment meaning the cost of production is reasonable [4]. Although it is cheap and relatively abundant, comparing it against some other semiconductor materials highlights some of its weaknesses, that become more apparent and as chip technology matures. As seen in Figure 2, the specific on-resistance of the material versus breakdown voltage on a log-log graph points it as the least desirable material;

the closer the material is to the south-east corner, the higher its performance will be [5].

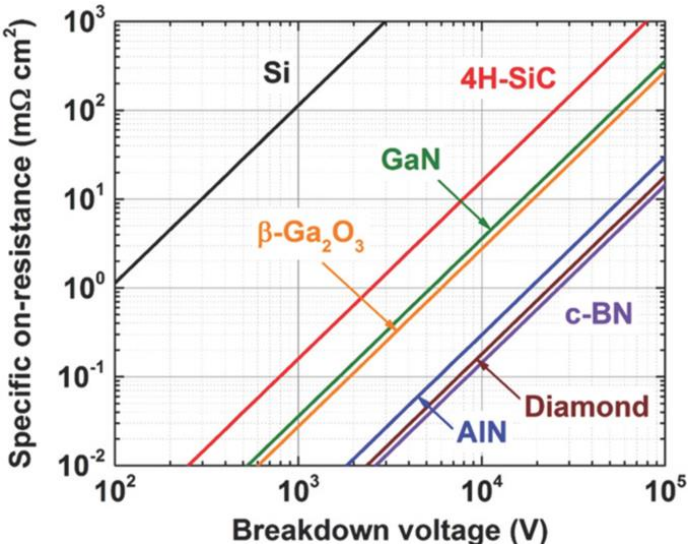

Figure 2: Log-log Baliga constant contours figure-of-merit for a range of semiconductors *[5]*

Even though the composition of a silicon wafer is consistent of mostly pure silicon, there is a requirement for small amounts of impurities for enabling it to conduct current. This is because in the standard diamond crystalline structure of the wafer, each silicon is bonded to another 4 atoms, leaving no valance electrons. By replacing some of these atoms with either a group 13 or group 15 atom (e.g., boron and phosphorous respectively), the addition of the extra electron or a lack thereof can allow for their transfer around the structure. Semiconductors with negative charge carriers (electrons) are referred to as “n-type”, whereas those with positive charge carriers (holes) are “p-type” [6].

2.2.1.2 Silicon Carbide

Silicon Carbide (SiC) is a more recent material that has gathered attention as a wafer material, proving especially useful for devices where withstanding harsh conditions is necessary. For lithography purposes, the strong chemical stability of SiC makes etching more difficult. The material has however seen being used for additional functions in microelectronic device fabrication, such as the sensing layer, biocompatible coating as well as the buffer layer [4].

There are many different varieties of SiC, with differences in the layout of carbon atoms within its crystalline structure. Among the many different types, 4H-SiC is one of the more common, particularly used for high-temperature electronic devices, ultra-

high precision micro and nano-dies as well as other applications. The material 6H-SiC is also commonly used, finding applications in transistors for the manufacture of optoelectronic devices [7]. The denomination “4H” or “6H” refers to the stacking sequence of carbon within the structure, characteristic of a zig-zag pattern [8]. As there are many more sequencing patterns of the material available, it is important to recognise specific applications of each structure in order to choose the correct material for each application.

2.2.2 Silicon Dioxide

On top of the conventional materials of photolithography, some additional materials are used to optimise the device structure. Some processes require a thin silicon dioxide (SiO_2) layer formed on top of the silicon substrate, as it can act as an insulating layer between conductive regions due to its relatively large band gap of 9 eV [9]. Such SiO_2 layers can also be applied as hard masks for etching the substrate below, and tend to have significantly higher etch resistance than most resists [10].

The SiO_2 layer is commonly formed by the process of plasma enhanced chemical vapour deposition (PE-CVD), and a variety of different reaction schemes can be used. Silane and oxygen are some of the more common reactant molecules for CVD in this process, interacting as follows:

$$SiH_4 + O_2 \rightarrow SiO_2 + 2H_2$$

The oxygen can be replaced by other oxide agents such as N_2O, NO and CO_2 [10]. The SiO_2 layer is formed on top of the substrate before the photoresist layer deposition.

2.2.3 Positive and Negative Tone Photoresists

There is a large range of photoresist materials available on the market, which can be divided into two main categories as mentioned, negative and positive tone resists. For positive tone photoresists, the exposed region is soluble to the developer, whereas for negative tone resists, the unexposed regions are dissolved.

Among the different polymeric resists available on the market, the chemistry dictates the properties of the material. Among them are epoxy based resists such as SU-8 for electron beam lithography, which increases the stability of the film by cross linking the polymer films and makes the material more rigid [11]. Many advances have been made in resist materials and EUV lithography, which uses wavelengths of 13.5 nm,

with the potential of improving the resolution of the pattern as dictated by the Raleigh formula [12]. Novel inorganic nanocomposite photoresists are seen as one of the candidates to realise the full potential of this technology [12].

Positive and negative photoresists both have benefits and drawbacks, for example the relative cost, adhesion to the substrate, minimum possible achievable feature size and etch resistance. There are seemingly also some inherent limitations of the resists, such as negative tone resists swelling during development, limiting the achievement of very small feature sizes [13].

2.3 Nanocomposite Photoresists

Nanoparticles are dispersed in the resist which acts as a matrix to separate and support them. Generally, the nanoparticles are formulated by the reduction of salts in a solution and form the nanoparticles. The method can either be in-situ or ex-situ. In the ex-situ method, the nanoparticles are formed following the addition of the colloidal nanoparticle solution to the photoresist. For the in-situ method, precursors to the nanoparticles in solution are added to the photoresist, which relies on them being formed post infiltration [2]. The main disadvantage of these methods is that the nanoparticle solvent is not always necessary compatible with the resist in laboratory conditions. The functionality of the nanofillers within the resist material extends beyond the lithography process (such as enhancing the electrical reinforcement and plasmonic resistance [14]), however the increased etch resistance along with mechanical reinforcement will be the focus of this review.

2.3.1 Inorganic Nanoparticle Fillers

The effect of adding nanoparticles to enhance the etch resistance has already been proven, such that in the case of metal-oxide nanoparticle-based photoresists, which had successfully solved the problem of overcoming the limit of transferring of the pattern onto the substrate surface for a node smaller than 30 nm [15]. Smaller nanoparticles can also lead to stronger results due to a higher effective surface area, and ability to act on the ever-shrinking feature-size of the photoresist dimension. Nanoparticles from solvents have been able to reach small sizes of a few nanometres across; new techniques such as the MACS have shown promise in delivering small metallic clusters that may be applied to the photoresist [16].

2.3.2 Nickel and Nickel Oxide Nanoparticles

Nickel-nanocomposite photoresists have seen a fair amount of attention received by researchers and industries, as the metal has shown promising improvements to different parameters of the final semiconductors as well as the preliminary substances during the manufacture process. Carbon coated nickel nanoparticles implanted within a photoresist has seen the increase in complex dielectric permittivity of approx. 116% [17]. Similar results of helping the increase of dielectric constant by the use of nickel nanoparticles for semiconductors have been reported by [18], where it was used with composition with PVDF; the nickel could reportedly also be replaced with other metals such as aluminium, stainless steel or copper.

2.4 Etching Processes

Plasma etching is a solvent free and selective method, where plasma produced radicals react with the substrate to create features. It is a dry etching method, which is considered simpler and cleaner compared to wet etching techniques. It can also enable higher etch selectivity of the substrate with respect to the mask [19]. Plasma gases are dependent on the substrate material, e.g. a mixture of SF_6 and O_2 is used in the case of silicon, which can yield high etch rate of the substrate [20]. The process occurs in a vacuum chamber, where the platen is impacted by the ions to react with the surface of the substrate.

2.4.1 Conventional Plasma Etching

In the etch chamber, there are multiple physical and chemical processes that contribute to the etching of silicon. These processes involve the interactions of various particles, including photons, negative and positive ions, neutrals and radicals [21]. First, the etch gases are introduced into the vacuum chamber, where the plasma is formed by ionisation. RF (radio frequency) power is used for striking plasma. A molecule (such as SF_6) reacts with an excited electron to create a positive ion and an electron as shown in the equation below.

$$SF_6 + e \rightarrow SF_5^+ + F + 2e$$

The SF_6 molecule can also undergo dissociation, creating neutral species, and ions in the plasma. SF_6 is thus a carrier of F radicals. The reaction for chemical etching of silicon using fluorine atoms is shown below [21].

$$Si\ (s) + 4F\ (g) \rightarrow SiF_4\ (g)$$

The reaction product SiF_4 is a gas and therefore can be easily pumped away and removed from the chamber during the etching process. Positive ions formed in the plasma reactions also impact the wafer surface. An acceleration action is driven by the negative platen voltage underneath the wafer, causing etching of the substrate and mask, physically. Chemical etching is dominant for removing the substrate material, whereas physical etching has a higher effect on the mask. Tool variables such as the RF power and the platen power are used to optimise the process as desired.

2.4.2 Bosch Process

The Bosch process for silicon etching is popular in the semiconductor industry, boasting very good etch selectivity with respect to the mask, and producing anisotropic feature shapes via DRIE (deep reactive ion etching). In general, the process alternates between deposition of CF moieties (for example as C_4F_8) on the surface of the sample, and the etch step where a fluoride radical plasma (for example SF_6) molecules attack the surface as shown in Figure 3.

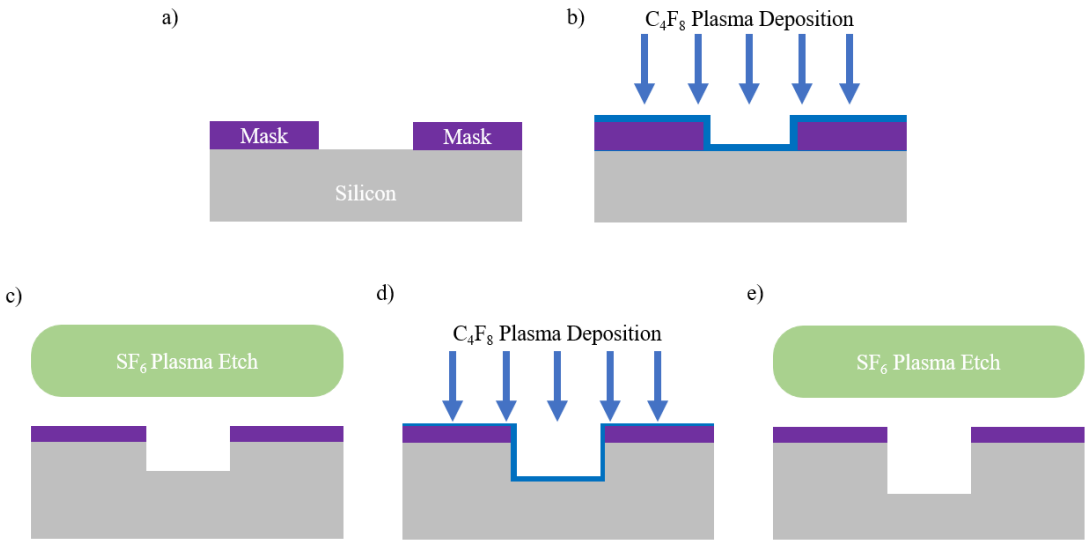

Figure 3: Diagram displaying basic principles of the Bosch process: a) showing a cross section of a wafer with exposed silicon; b) C4F8 layer is deposited on the surface of the wafer; c) the wafer surface is being etched with a bias on the horizontal faces of the pattern; d) secondary C_4F_8 layer is deposited; e) the passivation layer is again etched and the process is repeated for a set number of cycles.

The CF material serves as a protective barrier on the sidewall of the feature, which prevents the sidewall from being etched during subsequent processing steps. This results in an improved vertical profile for the trench. A vertical trench is desirable in

microfabrication processes as it leads to more controlled features with high aspect ratios.

The platen bias in the process is used to control the vertical direction of the ion bombardment, which also increases the etch rate. The nature of the process means that the effect of each cycle visible on the sidewalls of the trench, due to rounded edges being formed after each deposition and etch cycle [22].

The exposed silicon also favours reaction with the fluorine free radicals, unlike the mask, increasing the etch selectivity of this process.

3.0 Methods and Materials

3.1 Photoresist Formulation

3.1.1 Integration of Nanoparticles

Commercially purchased nickel nanoparticles were used for creating the samples in this series of experiments. With a large amount of material available, it was possible to create multiple resist samples with different combinations of resist and solvent, as well as different nickel loadings. This proved beneficial during the initial sample optimisation for the experiments, when samples created were found to be sub-optimal, due to issues such as agglomeration of nanoparticles. To create the resist sample, first the nickel nanoparticle powder (with quoted particle size in the range of 5-20 nm) was mixed with AZ EBR solvent (supplied by MicroChemicals) in the nanoparticle hood, after which it was brought into the lithography area. The suspended nanoparticles, in EBR was mixed with photoresist to create the sample solution. Ideally, the nanoparticles would be mixed with the resist without using EBR at all, as the solvent reduces the thickness of the final resist by diluting the active material, MIR-701 and makes the solution more viscus. Because there was no nanoparticle hood in the lithography area, it was impossible to mix MIR-701 with the nanoparticles directly without exposing it to UV radiation, i.e., the photoreactive material could become activated. This would have detrimental effects on the material before testing could occur. To avoid diluting the solvent in future experiments, a nanoparticle hood installed in a non-UV area would enable the nanoparticles to be integrated directly with the resist.

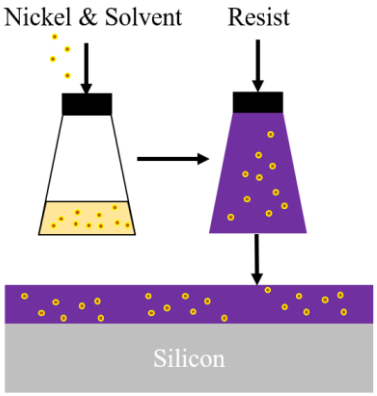

Figure 4: Diagram displaying how the nanoparticles are introduced into the photoresist. The nickel nanoparticles are first mixed with the solvent before the addition of the photoresist. After ultrasonication and settlement of the larger particles, the composite formulation is spin coated on the silicon substrate.

3.1.2 Loading of Nanoparticles in Resist

The loading of the nanoparticles relative to the photoresist generally depends on the type of nanoparticle, the size, the resolution of the patterns required and the desired outcome of the application. Most studies analyse a range of concentrations of the nanoparticles, such as 5-20% w/w of Hafnium-oxide Nanoparticles in aqueous PGMEA, which was applied by spin coating. The research team reported that the presence of the nanoparticles increased the etch resistance of PHOST 9-fold compared with a previous study [23].

The loading of nanoparticle is decided by the number of nanoparticles desired within the mask, and how narrow the desired etch structures are. Over-loading is an issue, since the agglomeration of nanoparticles can effectively reduce their impact as they are less evenly distributed within the photoresist. They will behave as larger particles would, thus reducing the effective surface area of the particles [24]. To alleviate this issue, ultrasonication as a dispersion mechanism could be used [25]. This method disperses the particles by cavitation action, where by microbubbles are formed and collapse, causing a pressure differential within the fluid and dispersing the particles across the medium [26].

3.2 Sample Materials

3.2.1 Silicon Substrates

To create the nanocomposite resist and the SiO_2 samples, 150 mm in diameter and 675 µm thick p-type wafers were used. The wafers were cleaved into approx. 3 x 3 cm pieces, so as to fit multiple tokens onto a single carrier wafer, to allow for testing of multiple formulations in one run. In later testing, whole wafers were used to analyse the different etching results, by removing the need for the use of carrier wafers and crystal bonding.

3.2.2 Photoresist

When selecting a photoresist material, various factors need to be considered, such as ease of use, stability, compatibility with etching conditions, and the ability to suspend the nanoparticles uniformly. An appropriate resist to solvent ratio is also important to achieve a high enough thickness before etching. For the majority of the tests, AZ MIR 701 positive tone photoresist was used. The photoresist was also compatible with the

AZ EBR solvent which was used to dissolve the nanoparticles in before the mixture was made.

3.2.3 Solvent

Samples of varying concentrations of AZ MIR-701 in AZ EBR resist were prepared to determine the highest quantity of the photoresist that could be blended with the solvent. The MIR-701 and EBR mixtures were spin coated onto silicon, after which the material was soft- and hard-baked and the thickness measured using the ellipsometer. A larger amount of the solvent would be beneficial during its mixing with the nickel nanoparticles, as with a higher volume dispersion medium there would be less chance for agglomeration at this early step in the process. Following tests, it was established that 1 gram of EBR per 25 grams of MIR-701 would be the most optimal amount.

3.2.4 Adhesion Promoter

Before the nanocomposite resist was placed on the substrate, the adhesion promoter TI Prime from supplier Microchemical GmbH was applied to ensure consistency throughout the experiments. The adhesion promoter is more crucial in the development stages of lithography, to ensure that the patterns adhere to the substrate during the process.

3.2.5 Nickel Nanoparticles

The nanoparticles used were purchased from ThermoFisher Scientific and came in the form of a powder. The nanoparticle size range was approximately 5 to 20 nm as stated by the manufacturer. A TEM image of the nanoparticles can be seen in Figure 5.

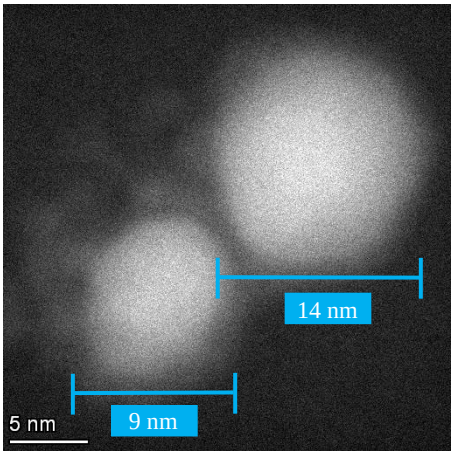

Figure 5: TEM image of the nickel nanoparticles used in the project. The nanoparticles were surrounded with an oxide shell on the surface (Image credit: Sean Lethbridge).

The nanoparticles had a NiO shell which passivated the nanoparticles during transport; the layer naturally forms when the powder is in contact with air [27]. The thickness of the NiO layer averaged between 0.5 to 1.5 nm as stated by the supplier.

3.3 Sample Preparation Process

3.3.1 Substrate Preparation

The same procedure was followed for the preparation of the samples for the duration of the project. The first step was to rid the substrate of organic impurities, which depended on whether the wafer box was freshly opened, or if the box was opened and closed multiple times. New out of the box wafers were treated in the Plasma Asher, Plasma Etch PE-75, with 10 sccm 02, at 90 W for 10 minutes. All other substrates were treated by the following process:

1. prepare an acetone bath for the substrate and ultrasonicate for 10 minutes;
2. transfer the substrate into an IPA bath and ultrasonicate for 5 minutes;
3. once the substrate is out of the IPA, dry the substrate using a nitrogen gun;
4. bake the substrate to dehydrate it on a hot plate at 150 ^{o}C for 15 minutes.

3.3.2 Dispersion of Nanoparticles

The process of dispersing the nanoparticles involved mixing the powder with EBR as described in section 3.1.1. After the resist formula was prepared, it was ultrasonicated 3 times for 10 minutes at 1 hour intervals. During the intervals, it was kept in the fridge. This process was necessary as the ultrasonicator warmed the resist formula, which increased the degree of agglomeration. When not in use, the resist was kept at temperatures between 1 to 3 ^{o}C as recommended by the manufacturer.

3.3.3 Positive Tone AZ Resist Preparation Procedure

A standard procedure was used to apply the resist onto the substrate. Even though the loading of nickel affected the thickness slightly, the spin speed of the tool was kept constant as the thickness was always sufficient for the etch process. The adhesion promoter TI Prime was applied after the dehydration step as described in section 3.3.1. The process was as follows:

1. prepare the hotplates for the baking step at 120 ^{o}C;
2. spin coat wafer;

    a. spin recipe set-up: Step 1: 4000 rpm, 1000 rpm/s acceleration, 20 seconds;
    b. pipette TI prime to cover wafer surface completely;
    c. start spin;
3. bake wafer at 120 ^{o}C for 2 minutes.

Following the solvent clean and the TI Prime process, the MIR 701 was applied:

1. prepare the hotplates for the baking steps at 90 and 110 ^{o}C;
2. spin coat wafer:
    a. spin recipe set-up: Step 1: 3000 rpm, 1000 rpm/s acceleration, 45 seconds;
    b. pipette 5 ml of MIR 701 photoresist to form a puddle in the centre;
    c. start spin.
3. Softbake wafer at 90 ^{o}C for 3 minutes;
4. Rest the wafer for 2 minutes to re-hydrate it;
5. Expose the wafer at 150 mJ/cm^3
6. Post exposure bake at 110 ^{o}C at 90 s

The sample is then ready for ellipsometry analysis followed by etching and a secondary ellipsometry analysis.

3.4 Etching Processes

3.4.1 APS SiO_2 Etch Process

The samples were tested with etch tools that were provided by the sponsoring company SPTS/KLA. The APS (Advanced Plasma System) is a dry-etch tool that uses a very aggressive plasma process to etch the resist. The APS system is primarily used for dielectric etch processes (SiO_2 and SiN) and SiC trench etching processes. The etch recipe selected was based on a standard SiO_2 etch, the recipe was shortened to suit the thin photoresist that was being tested. The primary etch gas SF_6 was used as the feed gas for the plasma, with the standard IWC (Inter Wafer Clean) process used in between samples. Cleaning the chamber in between the runs with the use of Oxygen removes the majority of impurities such as organics, which maintain constant conditions and helps to thus improve the reproducibility. The process parameters of the recipe can be seen on the following page in Table 1.

Figure 6: APS etch tool used in the project with a test sample loaded in the vacuum chamber. The sample is then transferred from the vacuum interlock into the process chamber, where a turbo pump activates and creates a high vacuum environment. The process gases are then introduced into the chamber, where the plasma is struck, and the etching process occurs.

Table 1: APS xSwan_SiC_R02 process recipe details

		1		2		3		4	
Process		Strike		Step 1		Step 2		Step 3	
Process Pressure	**mTorr**	[redacted]	[redacted]	[redacted]	[redacted]	[redacted]	[redacted]	[redacted]	[redacted]
Source Power	**Watts**	[redacted]	[redacted]	[redacted]	[redacted]	[redacted]	[redacted]	[redacted]	[redacted]
Platen HF Power	**Watts**	[redacted]	[redacted]	[redacted]	[redacted]	[redacted]	[redacted]	[redacted]	[redacted]
SF6	**sscm**	[redacted]	[redacted]	[redacted]	[redacted]	[redacted]	[redacted]	[redacted]	[redacted]
O2	**sscm**	[redacted]	[redacted]	[redacted]	[redacted]	[redacted]	[redacted]	[redacted]	[redacted]
Ar	**sscm**	[redacted]	[redacted]	[redacted]	[redacted]	[redacted]	[redacted]	[redacted]	[redacted]
He	**sscm**	[redacted]	[redacted]	[redacted]	[redacted]	[redacted]	[redacted]	[redacted]	[redacted]

3.4.2 DSi-v SF-6 Bosch Etch Process

The DSi-v equipment employed a vertical silicon etch process utilising the Bosch etch technique, which involves the use of C_4F_8 and SF_6 gases. Similarly, to the APS, the standard IWC was used in between experiments. The details of the recipe used are shown on Table 2.

Table 2: DSi-v xSwan_HighAspectRun0_R03 process recipe details

		1		2		3			4		
Process		Strike		Dep		E1			E2		
Process Pressure	**mTorr**										
Source Power	**Watts**										
Platen HF Power	**Watts**										
O2	**sccm**										
Argon	**sccm**										
SF6	**sccm**										
C4F8	**sccm**										

3.5 Measurement and Characterisation

3.5.1 Ellipsometry Analysis

Ellipsometry is a non-invasive method of measurement which uses polarised light to determine the thickness and optical parameters of thin films [28], as shown in Figure 7.

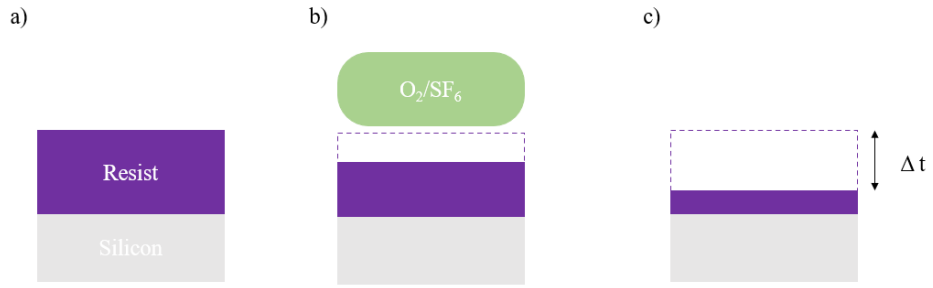

Figure 7: A schematic of the etching process showing measurement of resist thickness to calculate the etch rates. The resist is a) spin coated on the substrate, and then b) etched with a SF_6 dielectric etch, or a Bosch process etch, depending on the etch tools. The difference in thickness between the start and end of the process, as shown in c), is the variable which allows for the calculation.

This method was very important for the calculation of the etch rates, as the tool allows for the measurement of the thicknesses before and after the etch process. With the etch times, the etch rates could then be calculated. A diagram showing working principles

of ellipsometry can be seen in Figure 8. As the technique uses the interface of light reflected from the surface of the film, and refracted through the film, error can arise depending on the material that is being measured. For example, particles and nanoparticles can cause light to scatter. In general, elypsometry can accurately measure film thicknesses even with surface and bulk inhomogenous materials [29]. The magnitude of uncertainty is dificult to estimate, however using a model with low reported error as reported by the elispometry software should help to minimise this. SEM can also be used to verify film thicknesses against the model. Taking multiple measurments of the sample and creating a thickness map (such as in Figure 11) helps to estimate the uniformity of the layer and the etch process.

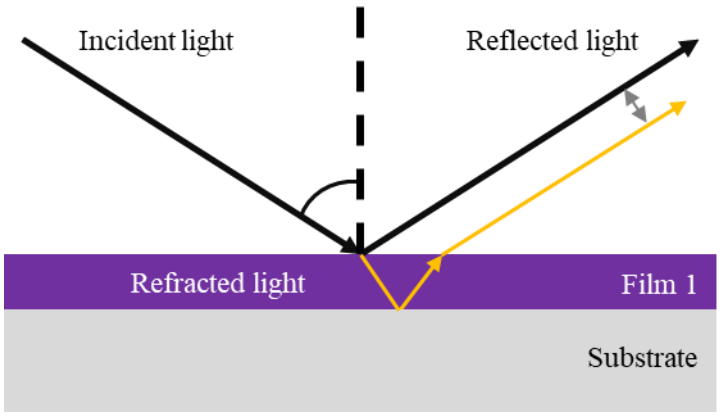

Figure 8: A diagram displaying how the ellipsometer determines film thickness. A light is shone at a known angle at the film, with some of the light reflecting and the rest refracting into the material. The light received back by the sensor is compared with the reflected light, and the film thickness can be calculated using the refractive index.

3.5.2 SEM & Digital Microscopy

Electron microscopy (SEM, TEM) are the most common tools to analyse images of nanocomposite photoresists, as they can operate at very high magnification meaning small nano-scale details can be analysed. It can be used to view how the nanoparticles are distributed across the surface of the photoresist especially from the top view, however the sample can also be cleaved through its cross section to examine how the nanoparticles agglomerate as a function of depth in the photoresist.

Digital optical microscopy was used alongside SEM to view the samples from a wider perspective. The tool allowed inspection of the samples for larger agglomerates and

analysis of the sample process optimisation. An image taken using a digital microscope can be seen in Figure 9, where agglomerates and resist can be clearly seen.

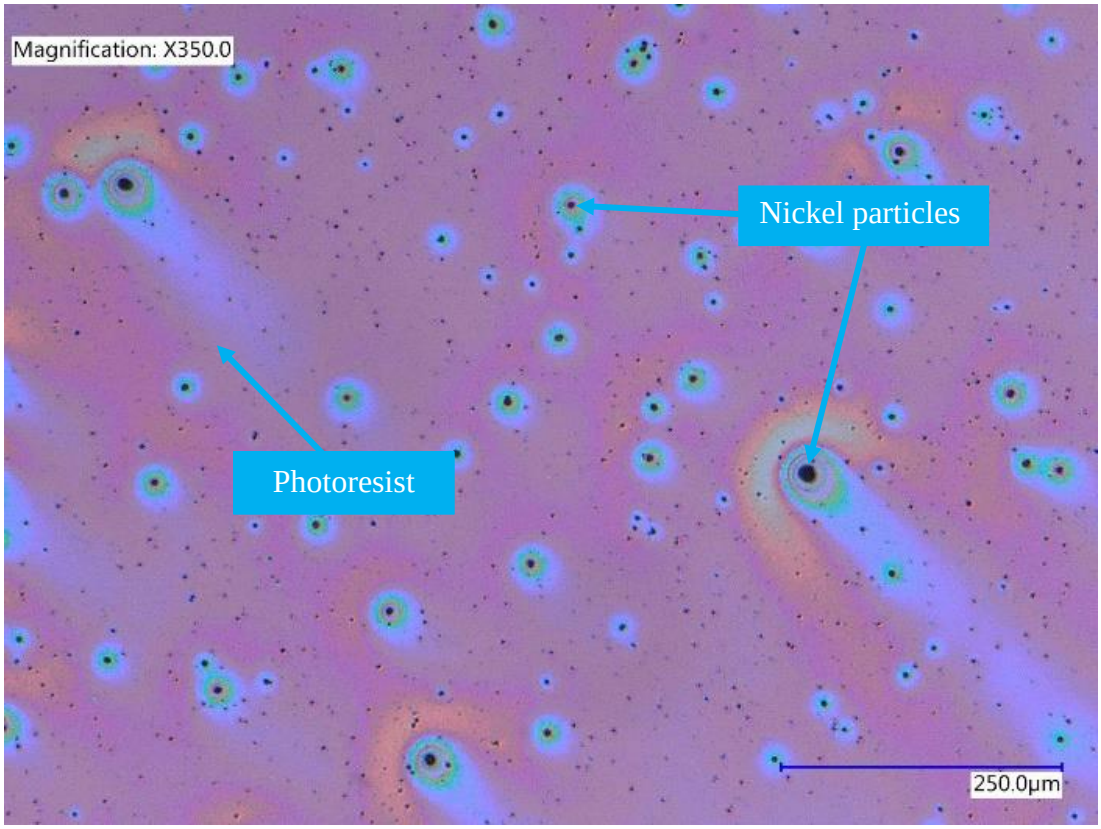

Figure 9: A digital microscope image showing nanoparticle agglomeration on the surface of the resist. The degree of agglomeration affects the thickness uniformity across the samples as indicated by the changing colours of the resist.

4.0 Nickel Nanocomposite Resist Etch Rate Results

This chapter presents the main experiment results which were obtained in two SPTS plasma etch tools, the APS (Advanced Physical Source) and the DSi-v (Deep Silicon – [extra] Volume). The experiments have two main objectives: first, to analyse the etch rates of the nanocomposite resists with different loadings, and second to compare the outcomes between the different etch processes of the high aspect Si etch process in the DSi-v etch module, and a SiO_2 etch recipe in the APS module. The results are compared between the different experimental set-ups to suggest reasons for the differences that arise. The samples were also analysed by SEM.

4.1 Sample Optimisation and Design

In the first set of experiments, 30 mm by 30 mm tokens coated with nanocomposite resist were adhered to the silicon carrier wafer using crystal bonding. Using smaller tokens allowed for use of a smaller volume of nanocomposite photoresist and conducting more experimental repeats. However, the primary benefit of this technique was that various loading concentrations of nickel photoresist formulations could be tested in a single run, ensuring that the chamber conditions of the etch tool had a consistent effect on all the samples. While the platen power, plasma coil power, substrate temperature, gas pressures and the ESC (electrostatic chuck) voltage were controlled by the automatic systems of the tools, the temperature margins, inside the chambers varied between the runs. Also while the inter wafer cleans were conducted in between experiments, certain other factors could potentially affect the results inside the APS, as discussed later in this analysis. In the initial round of experiments, the samples were positioned on a bare silicon substrate, given that the etched silicon is comparatively non-volatile.

Employing a blend of SF_6 and O_2 plasma during etching results in the formation of SiF_4, along with some other unstable species [30]. Etch processes are developed based on percentage of exposed etch material on the wafer surface. The standard SiO_2 etch recipe used is based on approximately 20% exposed SiO_2 material. The remaining surface area would be a photoresist etch mask. In all subsequent experiments, the carrier wafer was coated with MIR-701 photoresist and an SiO_2 token was added for comparison purposes. Figure 10 shows the sample set-up of later experiments, with photoresist tokens and SiO_2 in the middle.

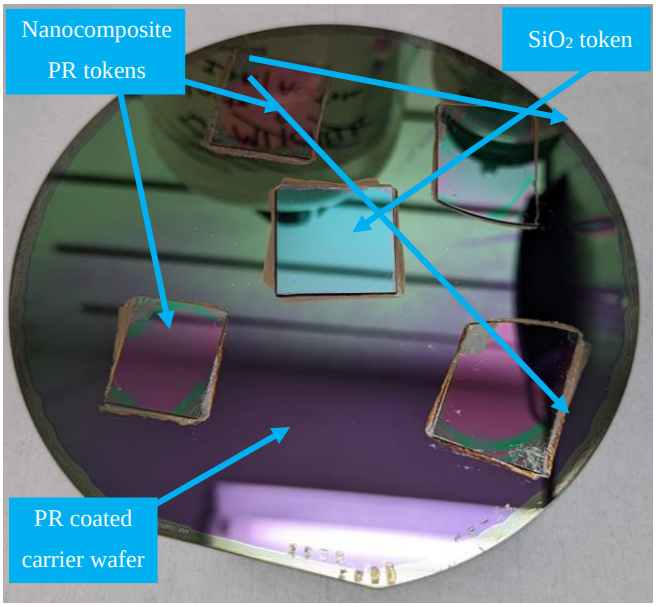

Figure 10: Experimental set-up of nanocomposite resist token pieces on a carrier wafer. Each token has a different concentration of nickel present, with one token containing no nickel in the photoresist. The carrier wafer was covered with photoresist, as it would reduce the presence of species created when the etch gases react with exposed silicon.

The carrier wafer was coated with the resist for the purpose of representing open area of a typical whole wafer setup. It reduces the Si reaction products such as SiF_4, and thus removes the possibility of such species reacting with the nickel in the photoresist.

4.1.1 Token Sample Preparation Process Flow

The preparation of the nanocomposite tokens started with cleaving a silicon wafer into small pieces, after which the cleaning and resist application process was conducted that is explained in the Methods and Materials section. Each token contained different a nickel nanoparticle loading, with one sample containing no nickel; this acted as a control. For later experiments, an additional SiO_2 token was added for comparison purposes. A standard inter wafer clean was conducted in between the actual runs to reflect workflows occurring in the industry, and to ensure that the chamber is maintained in a stable state before each run.

4.1.2 150 mm Substrate Preparation Process Flow

For the 150 mm substrate, the whole wafer was introduced into the etch tools which removed the need for the carrier wafer and crystal bonding. This however introduced the potential for differing conditions in the chamber due to either temperature variations or contamination within the chamber. For this reason, the sequence at which

different nanoparticle loading wafers were etched was randomised with two fully covered resist wafers tested before and after the experiments. The sequence of the experiments can be seen in Table 6 and Table 7 in the in-depth results analysis section 4.3. Assuming no contamination, the control, nanoparticle-free resist wafers were expected to provide very similar etch rate results. A standard inter wafer clean was conducted between each of the wafers, with extended clean times following the testing of the last samples.

4.1.3 Etch Tool Plasma Uniformity Check Analysis

The nickel resist experiments require the measurement of thickness before and after the etch to analyse the etch resistance of the material. Due to the set-up of the initial experiments, with the use of tokens on a single 150 mm substrate, it was important that the tool etched the material uniformly across the plasma contact area. Checking for the etch uniformity also gave an important insight into the operation of the machine and helped to understand the scale of error that could be possible between the results. The analysis was conducted by creating a test sample followed by pre- and post-etch thickness measurements. The test sample was a 150 mm Si wafer with a photoresist (MIR-701) layer spin coated onto the surface. A photoresist layer without Ni nanoparticles was used, as the presence of Ni could increase the error of the ellipsometry readings. The ellipsometer relies on light refraction through the resist layer, meaning that light absorbing species (e.g., Ni) could cause issues when searching for variations on this scale. The 13-point test was used which took readings on a large segment of the wafer, in a pattern as shown by Figure 11.

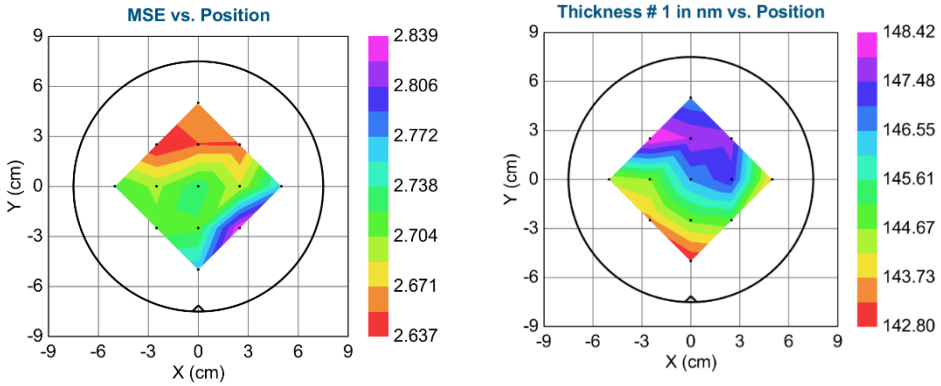

Figure 11: Example of data output for ellipsometry analysis of a 150 mm wafer undertaking a 13-point test. The ellipsometry analyses each of the datapoints for thickness and returns the MSE depending on the degree of diffraction of the light. Higher thicknesses and agglomeration increase the average errors.

The ellipsometry tool provides a range of data aside from the thickness of the resist layer, such as the estimated error and the raw data associated with each of the readings. The results analysis involved calculating the difference between the maximum and the minimum value to calculate the range of the result, as well as the standard deviation. Additionally, the average etch depth was calculated to find out the range of the results as a fraction of the actual etch conducted. The results can be seen on Table 3 and Table 4 for the APS and DSi-v etch tools respectively.

Table 3: Etch uniformity results on the APS from a 13-point ellipsometry test pre- and post-etch

Max – min etch depth /nm	3.25
Std. dev.	0.88
Avg. etch depth /nm	161.91
Max-min as % of avg.	2.0 %

Table 4:Etch uniformity results on the DSi-v from a 13-point ellipsometry test pre- and post-etch

Max – min etch depth /nm	12.94
Std. dev.	3.86
Avg. etch depth /nm	452.67
Max-min as % of avg.	2.9 %

Overall, data from the APS showed more consistent results compared to with the data from the DSi-v, with a lower value of standard deviation as well as the difference in range relative to the etch rate. The overall error for both however appears relatively low, with 2.0 and 2.9 % for the APS and the DSi-v respectively. The DSi-v uses the Bosch etch process which includes a polymer deposition step, this could be a possible explanation for the lower uniformity. The process must account for depositing the CF_4 radicals uniformly across the surface, as well as distributing the plasma evenly in contrast with the APS that only consists of the plasma etch stage. However, without a larger number of tests the difference could be due to natural errors and small sample size. This experiment highlights the weakness of using tokens on a carrier substrate, as the sectors of where the samples are placed could affect the results, especially in the DSi-v. However, conducting multiple test runs should reduce the effect of this error. Using a whole nanocomposite resist covered 150 mm substrate should be better still, as there will be a lot more datapoints from a single loading sample to reduce this error.

4.2 Token Nickel Resist Etch Rate Experiments

4.2.1 APS Etch Rate Results

The first experiment conducted involved testing Si tokens in the DSI-v with different nanoparticle loadings in the PR coating of each token, loadings ranged from 0 to 100 mg per 25 grams of resist (0 mg/g to 4 mg/g). The main goal of this experiment was to analyse the loading to etch rate relationship, and to find whether the amount of nickel was enough to make noticeable changes to the etch rates. The measured etch rates can be seen in Figure 12. Although all runs demonstrate that the loading of nickel has a beneficial impact by reducing the photoresist etch rate, significant differences in etch rates can be noted across the runs. The runs were conducted in a sequence as indicated by the letter series, with the first experiment being 2a, followed by 2b and 2c. The etch rates vary significantly between the series, even for the control sample with no nickel nanoparticles. The result 2b may have been affected by an issue with the run which made the etch rate of the 25 mg token unreadable. The last run 2c showed virtually no improvement of the etch rates with additional nanoparticle loading.

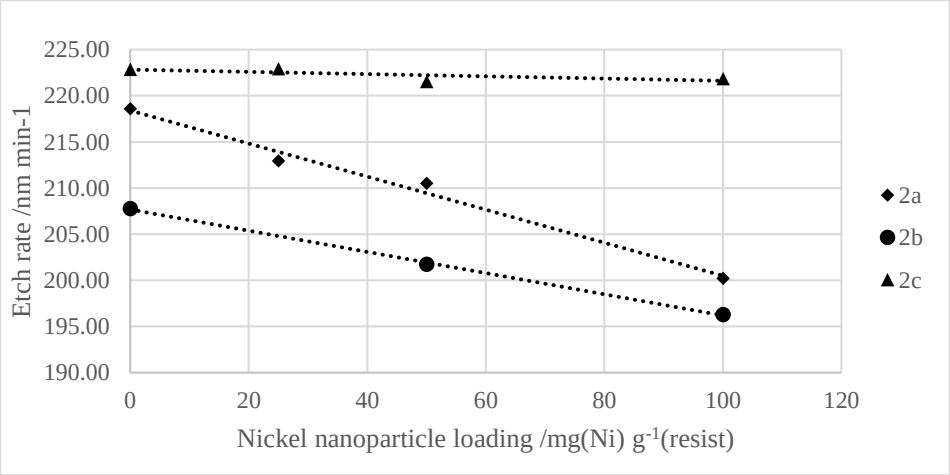

Figure 12: APS etch process on 3 separate carrier wafers 2a, 2b, 2c, with each one carrying a set number of samples. Experimental set-up used can be seen in Figure 9.

The first experiment suggested that there is potential for improving the etch rates by introducing the nickel nanoparticles into the resist, however the results were not repeatable. This was one of the reasons why the following experiments were also conducted in parallel in the DSi-v as well as in the APS. Also, the carrier wafers were

covered with nanoparticle free resist material before the tokens were bonded, to make sure that the material reacting with plasma would be limited by covering the open surface of the silicon.

The second experiment using the Si tokens photoresist samples showed more consistent results as shown by Figure 13, however they still displayed some variation between the runs. The overall trend shows an improvement in the etch rate with increasing nickel loading in the photoresist. The experiment was conducted 3 times. The average etch rate of the samples was much lower compared to the initial experiments; this could be due to coating the carrier wafer with the photoresist. Figure 13 b) shows that the first experiment 4a displayed a clear etch rate improvement on Ni addition, followed by a significant plateauing of the results for runs 4b) and c). This occurred despite using a more thorough inter wafer clean between the experiments.

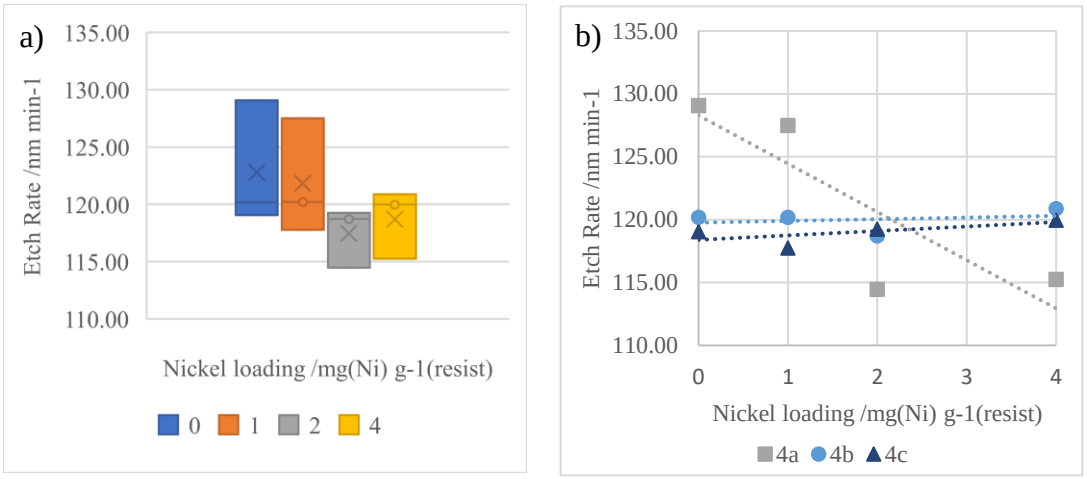

Figure 13: Comparison of different nanocomposite resist concentrations with the process APS xSwan_SiC_R02. a) Box and whisker plot of etch rates for multiple repeats of samples of set nanoparticle concentrations in the APS; b) scatter chart showing the data as a series of each run.

The results in Figure 13 show the contrast of how the results change with each successive experimental run. Only the result from experiment 4a) shows an improvement of etch resistance of the material with increasing Ni loading, with the remaining results showing a constant etch rate. In addition, the etch rate of 2 mg/g resist appears to display marginally higher etch resistance compared to the higher loading 4 mg/g sample. This could be possibly caused by the positioning of the PR coated token Si samples bonded onto the carrier wafer. The overall results suggest that the conditions inside the tool have changed following the first experiment.

4.2.2 DSi-v Etch Rate Results

Comparatively, the results obtained from the DSi-v experiment were significantly more consistent than those of the APS experiment. A pattern is evident, namely that an increase in the nanoparticle loading in the resist leads to a decline in the etch rate. Figure 14 displays the outcomes, which incorporate data from three separate runs. The etch rate improvement is not visible for the 1 mg/g loading sample, however the higher loading 2 and 4 mg/g show a clear improvement in the etch resistance of the material. The results may suggest that there is a critical mass necessary for the nickel to have visible impact in the results, however this conclusion should be only considered after more data is obtained. The SiO_2 sample can also be seen in Figure 14 a), which was used as a benchmark for comparison as it is a very effective hard mask that is used in industry. The inclusion of the SiO_2 sample in the graph makes it difficult to observe the trend of the nickel loaded samples. However, it clearly shows the difference between the nickel-composites and the target material at this stage.

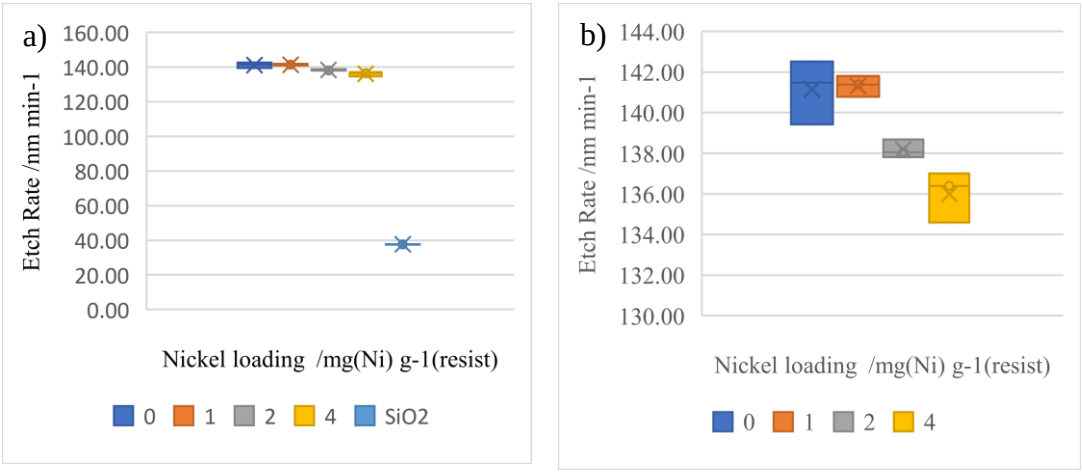

Figure 14: Box and whisker plot of etch rates for multiple repeats of samples of set nanoparticle concentrations in the DSi-v; comparison of different nanocomposite resist concentrations with the process DSi-v xSwan_HighAspectRun9_R03. a) and b) showing the results with and without the SiO_2 sample respectively.

4.3.3 Comparisons between APS and DSi-v Results

The same experiment involving token wafers on a carrier substrate has been carried out on both the APS and the DSi-v. Both processes showed some similar trends, and both showed some strengths and weaknesses within their processes. The APS can provide higher plasma density and platen power compared to the DSi-v in the tests conducted for experiment optimisation purposes. The results from the APS process

were not very reproducible; the sequential progressive change in the results suggests that there may be an issue with the chamber, causing differences between the experiment conditions. The APS also shows an increased relative etch resistance due to nickel loading in experiment 4a compared to the results from the DSi-v. Even though the APS shows less consistency in the results, it presents evidence of higher efficacy ratio for etch resistance due to the loading of the nickel. The standard deviation differences of the results can be seen in Table 5.

Table 5: Standard deviation values for both the APS and the DSi-v following the Si token nanocomposite PR experiments.

	Standard Deviation	
Nickel loading /mg g^{-1}	**DSi-v**	**APS**
0	1.58	5.48
1	0.51	5.07
2	0.45	2.62
4	1.26	3.03
Average	**0.95**	**4.05**

Some of the shortcomings of the APS results regarding consistency in the results are challenged by the results from the DSi-v, which shows a much narrower range for the specific loading amounts of nickel in the resist. The DSi-v tool shows it is true that nickel has the potential to affect the etch resistance significantly for the amount of nickel nanoparticles, and that the results show a trend by which the etch resistance increases along with additional nickel loading.

4.3 150 mm Wafer Nickel Resist Etch Rate Experiments

In the final series of experiments, large samples were individually tested in the etch tools to ensure that the outcomes were not impacted by consecutive material build-up. Given that the probability of material accumulation influencing the findings became evident after the token resist experiments, the resist testing sequence was randomised. The main disadvantage of this method is that it took significantly longer to prepare and test the samples, which provided fewer repeat runs compared to the token method. On the other hand, using a fully covered resist wafer increased the certainty of the results that were provided, not only because additional variables are removed, but also because the larger sample size allows for a more detailed ellipsometry thickness measurement. Due to the small token size, the samples in previous experiments were

measured using a 5-point test which tested an area of approximately 2 cm in diameter. The fully covered resist wafers were a lot larger and allowed for a 13-point measurement test which also was more compatible with the substrate shape. A 13-point test enabled a significantly more detailed thickness profile of the resist, which was used to confirm the uniformity of the etch in the different tools.

4.3.1 APS Etch Rate Results

The results in the APS show very little to no improvement in the etch rates as a function of the loading of the nickel in the resist, with very high variation in the control resists before and after the nickel runs. The results can be seen in Figure 15, which further suggests that the results from the APS are not accurate due to some issue with the process or the tool. A standard inter wafer clean process was carried out between the samples, and deeper O_2 clean processes before and after the experiment. The sequence at which the samples were etch tested is shown on Table 6. The 4 mg/g sample was tested first after the initial control sample, which interestingly has displayed better etch resistance compared to the 10 mg/g sample. This is not a result that would be ordinarily expected, as shown by the token etch rate experiments conducted previously. The etch rate appears to marginally improve for the 20 mg/g sample, but not as significantly as would be expected for the relatively high amount of nickel nanoparticles.

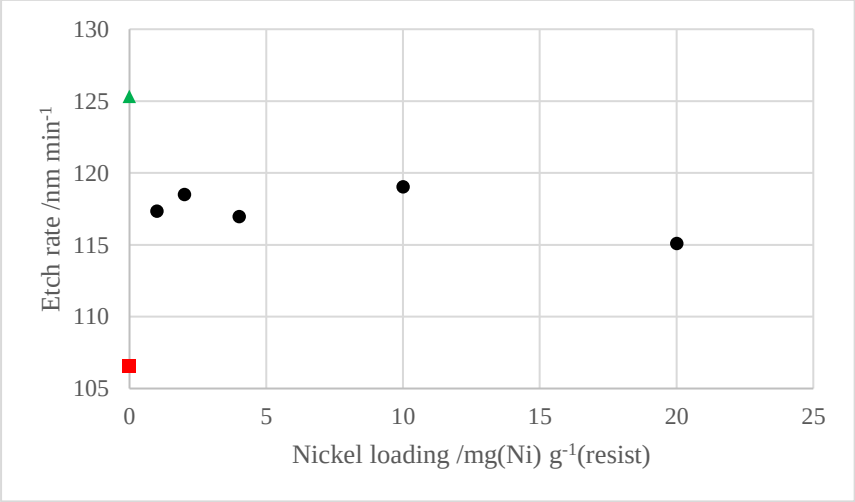

Figure 15: APS Etch Rate Results with Coated 150 mm Substrates. Scatter graph showing an experimental run where two control samples of no nickel are run at the start (green triangle) and at the end (red square) of the experiment in the APS. The remainder of the samples were tested in a random sequence.

Considering that the highest loading sample was tested last before the second control sample, it may have played a significant role in skewing the result by such a high margin. It could be the case that with only one clean cycle present between the two samples, it may have affected the chamber conditions for the second control. On the other hand, the second highest loading sample of 10 mg/g was tested before the lower loading 1 and 2 mg/g samples, the results of which do not appear as far outlying as the second control sample.

Table 6: Experimental sequence of fully covered resist wafers testing in the APS, including the etch rates of the PR as well as the etch resistance % improvement rate over the initial control sample (1-[sample etch rate]/[sequence 1 control sample etch rate])

Sequence	**Nickel Loading /mg g^{-1}**	**Etch Rate /nm min^{-1}**	**Improvement over initial control**
1	0	125.31	0.00%
2	4	117.32	6.38%
3	10	118.50	5.43%
4	2	116.94	6.68%
5	1	119.02	5.02%
6	20	115.08	8.16%
7	0	106.55	14.97%

4.3.2 DSi-v Etch Rate Results

The results in the DSi-v showed a much clearer trend compared to the APS, as was the case with the token experiments. A clear relationship was found - a higher etch resistance as a function of nickel increased loading in the resist. The results also showed a lower difference between the control resist test results obtained before and after the experiment, with the latter being lower than the 1 and 2 mg/g samples. The results for this experiment can be seen in Figure 16.

The difference in the etch rate results of the control samples suggest that some degree of material accumulation could take place, however this may also have been caused by chamber temperature variations. The higher loading Ni samples (10 and 20 mg/g) however show a marked and unambiguous improvement in the etch rate, suggesting a linear relationship between the loading and etch resistance in that regime.

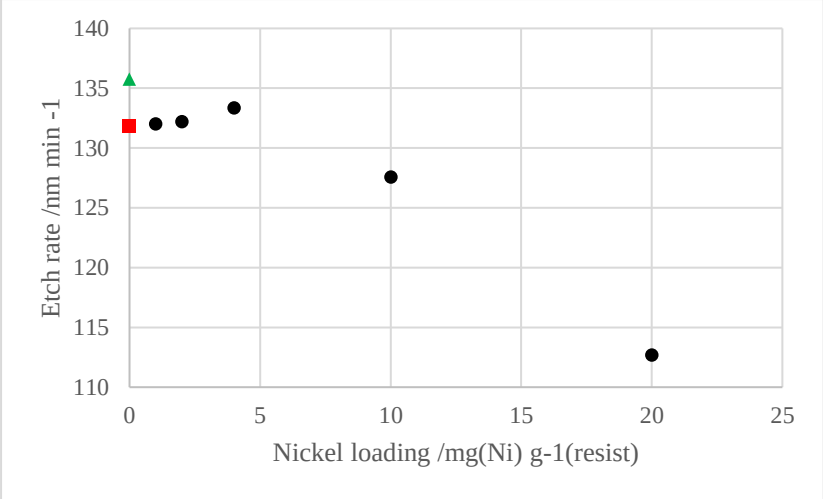

Figure 16: DSi-v etch rate results with coated 150 mm substrates. Scatter graph showing an experimental run where two control samples of no nickel are run at the start (green triangle) and at the end (red square) of the experiment in the DSi-v. The remainder of the samples were tested in a random sequence.

Table 7 below shows the sequence in which the samples were entered into the DSi-v, with an inter wafer clean in between each sample. The samples 1 and 7 in the sequence were the control samples, annotated by green and orange in Figure 16 respectively. The results fit with the assumption that the sequence at which the samples are tested plays a role, possibly due to material accumulation in the chamber. However more repeat runs would likely be necessary to see the pattern more clearly in the region between 0 and 4 mg/g. More repeats would also be desirable to determine the quantitative error from the ellipsometry measurements.

Table 7: Experimental sequence of fully covered resist wafers testing in the DSi-v, including the etch rates of the PR as well as the etch resistance % improvement rate over the initial control sample (1-[sample etch rate]/[sequence 1 control sample etch rate])

Sequence	Nickel Loading /mg g^{-1}	Etch Rate /nm min^{-1}	Improvement over initial control
1	0	135.75	0.00%
2	4	132.01	2.75%
3	10	132.21	2.61%
4	20	133.36	1.76%
5	1	127.56	6.03%
6	2	112.69	16.99%
7	0	131.80	2.91%

4.3.3 Discussion

The experiments conducted with the fully covered wafer resist were useful in establishing a correlation between the etch rate and the concentration of nickel nanoparticles. Furthermore, these experiments confirmed that there was no clear effect of Ni when the APS was used. A possible positive overall trend was overshadowed by the difference of the control results before and after the experiments. The DSi-v results did however show a trend of improvement in the etch resistance as the loading of nickel increases. Additionally, the results from the DSi-v suggest that a critical mass of the nickel nanoparticles (10 and 20 mg/g) may be necessary before the trend becomes linear, or even observable.

The results show promise for the new Ni nanocomposite material It is likely that the efficacy of the nanoparticles would improve once the process is further optimised. Clearly precise control of the etch environment is necessary for reliable testing.

4.4 Scanning Electron Microscopy (SEM)

SEM was used throughout this project to image the nickel nanoparticle resist samples. The images helped to confirm the presence of the nanoparticles and show their distribution across the resist. The images were utilised to measure the average size of the nanoparticles and compare with the information provided by the supplier. Prior to the etch tests, images were taken of the surface of the nanocomposite resist, an example of which can be seen in Figure 17. This image was taken from the lowest loading sample, which showed nickel nanoparticles of an average size of approximately 20 nm. The manufacturer stated that the particle size ranges between 5 and 20 nanometres. As the image only shows particles of 20 nanometres, we assume that the small particles may be too small to be identified in the SEM images. The image also shows that a degree of charging takes place when the beam is focused on a small area for a period of time (due to the non-conductive photoresist). This effect can reduce the quality of the image and make it more difficult to focus on the nanoparticles.

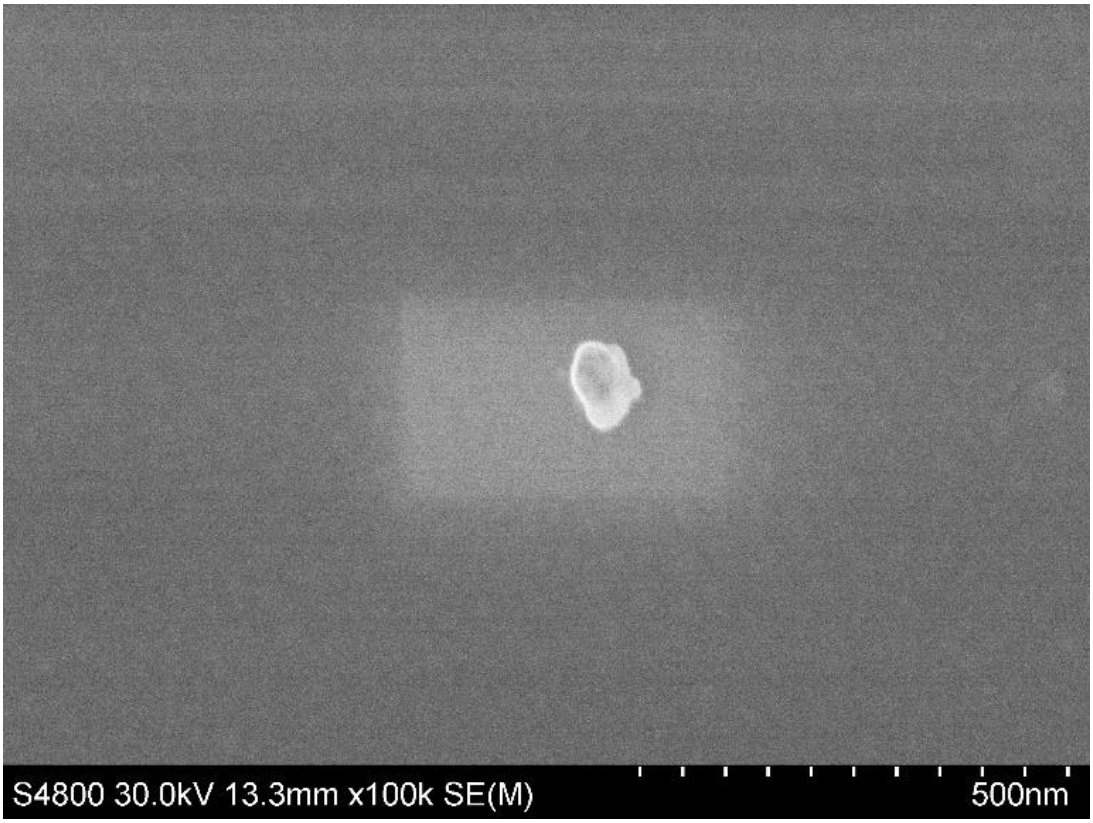

Figure 17: SEM image of a pre etch 0.2 mg nickel/g of resist sample. The image shows a sea of nanoparticles in the photoresist (the central particle is an impurity on the surface). The particles appear to be in a size range accurate to what the manufacturer described (4-20 nm in diameter), which also suggests a low degree of agglomeration of the particles.

The image displays a larger particle in the image's centre, which could either be contamination or an aggregate of nickel particles. This may be due to agglomeration occurring when the formulation rests in the vial before being spin-coated onto the substrate, i.e., after adding the nanoparticles to the resist.

The image shown in Figure 18 is a higher loading nickel nanoparticle resist that was taken post etch. The image shows significantly higher contrast than Figure *17*, as well as clear evidence of smaller particles. The image was taken at much higher zoom compared to Figure 17. It was much easier to focus onto images of nanoparticles post-etch. One of the possible reasons may have been that, given reduction of the thickness of the resist during etching, the nanoparticles could be accumulating on the surface of the resist and thus less of them were buried within the polymer matrix.

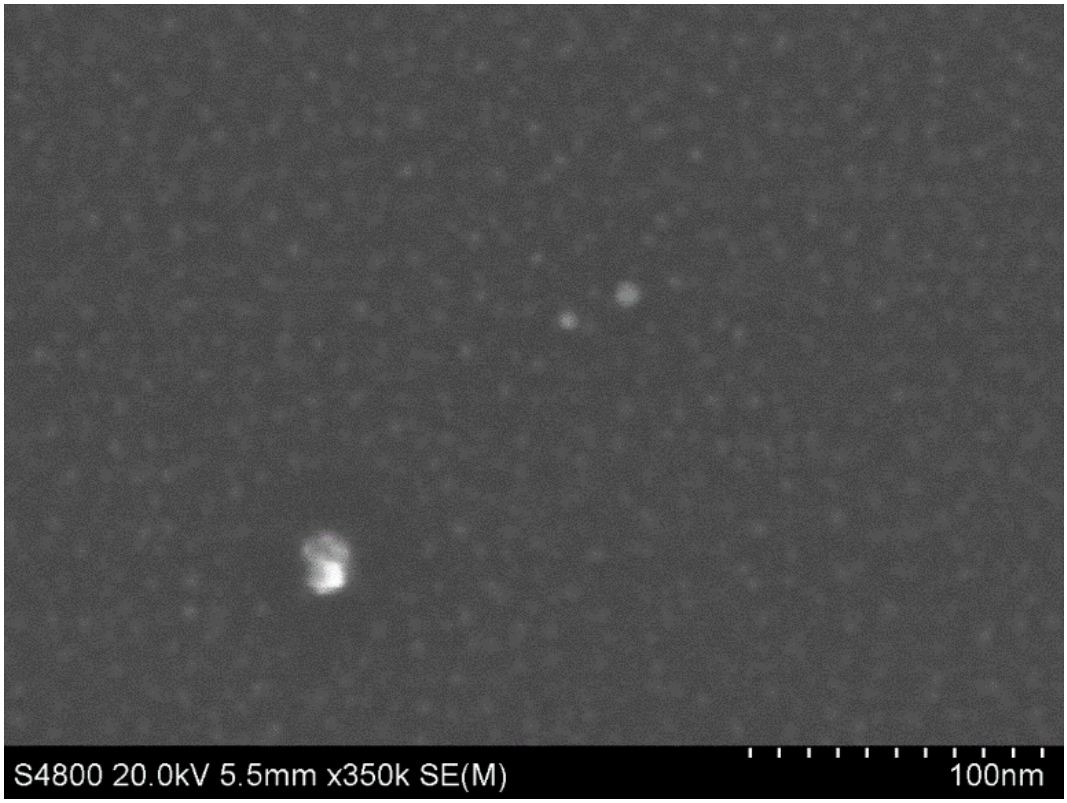

Figure 18: SEM image of a post etch 4 mg nickel/g of resist sample. Even though the image shows a similar result to Figure 17, the particles were much more apparent. This may be because the nanoparticles are submerged by a lower thickness of the photoresist and are left more exposed on the surface.

While both images show a clear a presence of nanoparticles in the samples, they appear to be of different size. Upon comparing the images, the charging and lower resolution of Figure 17 may be the cause of the particles appearing larger than they are in Figure 18. In both images however the particle size falls within the manufacturer limits and show relatively low amount of contamination or agglomeration. The correct distribution of nanoparticles is very important, especially if a resist is to be patterned with low feature sizes.

4.5 Summary

Overall, the results evidence for a strong relationship between the Ni nanoparticle loading and improved etch resistance of the nanocomposite resist, notably the experiments conducted in the DSi-v. These showed clear trends that could be interpreted as linear from the data that was available. The highest concentration nickel resists of 10 and 20 mg/g showed a very significant improvement in the etch resistance compared to the control samples, by 6 and 17% respectively. The initial results from

the APS show an even higher etch resistance improvement with respect to the nanoparticle loading of the resist, but subsequent tests showed the tool inconsistent results possibly due to the different etch chemistries. The sequencing of the samples plays a role in the etch resistance which is a lot more visible in the APS than it is in the DSi-v etch tool. Thus, the history of the sample environment appears to play a role. Unfortunately, it is difficult to estimate the error of the ellipsometry measurements due to the presence of the particles in the resist film, which affect the trajectory of light through the medium.

5.0 Conclusion and Outlook

5.1 MACS Nanoparticles

The Matrix Assembly Cluster Source (MACS) is a novel solvent-free method of producing and depositing nanoparticles in vacuum. This section will discuss the prospects of the MACS, to produce nanoparticles integrated into a resist and subsequently etch tested. The preliminary results will be discussed, as well as prospects for the technology when applied in the semiconductor industry. Future work will be needed to produce, characterise, and test different loadings of MACS nanoparticles embedded in the resist. The results described in chapter 4 can be seen as a reference for the long-term goal of creating novel nanocomposite resists by cluster beam deposition.

5.1.1 Introduction

The MACS is a new, versatile alternative to produce nanoparticles, finding applications where nanoparticles require to be a specific size, or when solvent free synthesis and deposition is desirable. The tool can produce nanoparticles that can be size controlled in certain conditions, and elemental or formed as a core-shell structure or a Janus structure [16], according to predictions. Several applications where the nanoparticles perform well have been found, e.g., catalysis where ultrafine cobalt clusters on carbon paper drive the oxygen evolution reaction [31] or silver and gold nanoparticles catalyse the of ozonation of nitrophenol waste water cleaning [32]. The

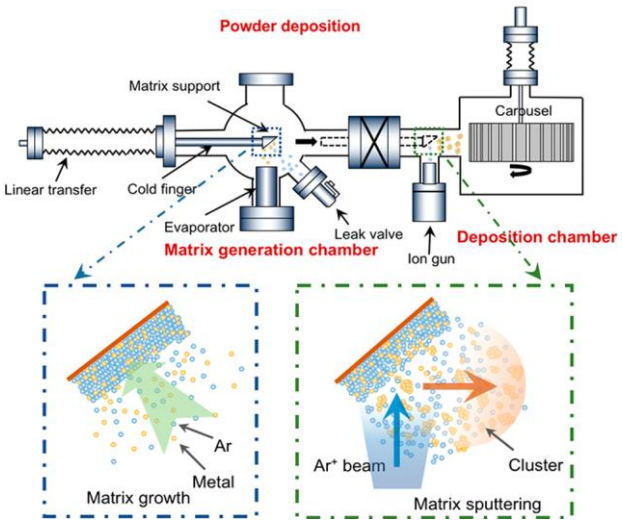

Figure 19: Diagram showing the MACS and its different components. The solid matrix is formed on the support in cryogenic conditions, after which the Argon beam is used to sputter the matrix and causing the cluster to form [16].

absence of ligands may allow for finding more efficient catalysts as well as the production of sensors and other functional devices.

Figure 19 shows an early version of the MACS (MACS I) which reveals how the clusters are created. Nanoparticles created by the MACS have the potential for application in the semiconductor industry. As the etch rate is the characteristic that is being tested in this project, nickel cluster production by MACS was identified for potential proof of principle experiments, with Ni being a material of interest in semiconductor manufacturing.

5.1.2 Methodology and Process Flow

In the MACS, the nanoparticles generated in a matrix are sputtered onto a dry support, such as a powder. The process for integrating the metal into the resist had to be modified as a result. The process that was chosen involved using the resist PMMA which, with the aid of a cross linking material, was turned from a positive tone e-beam resist into a negative tone UV resist [33] [34]. There is a selection of cross-linking materials that could be used for this purpose, however Irgacure 651 was used as it was found to be the most effective in the formulation of this resist material in literature [34]. Once the cross-linking material was mixed with PMMA and dissolved in Anisole, the slurry was mixed using the ultrasonicator for 10 minutes. This was a precautionary step to ensure improved dispersion of the material; while the cross linker dissolves well in the solution, there is a risk of agglomeration of the nickel nanoparticles. Irgacure 651 was added to the PMMA at 15% w/w ratio (weight of the cross-linker/total weight of PMMA + cross linker), as it was found to be the most optimal with respect to patterning quality of the final solution [34]. The process conceived for depositing the nanoparticles on the crosslinker prior to adding the material to the PMMA in solvent can be seen in Figure 20.

After the samples were created, they were tested in the DSi-v to mirror the previous nanocomposite resist experiments of chapter 4. The process in the DSi-v was kept the same as the previous experiments, with the exception that the number of cycles in the tool was reduced from 70 to 15. This was because PMMA has lower etch resistance compared to MIR-701, and the resist layer was thinner on the substrate. The whole 150 mm wafer was spin coated with the resist as the MACS nanoparticle doped cross linker PMMA material was abundant, and the experiment would be made more

reliable given the larger surface area for the ellipsometer readings. The experiments were conducted in the DSi-v exclusively rather than in the APS, as one of the conclusions of the previous sets of experiments was that the former tool may not produce accurate results. The control samples were created by mixing PMMA and the cross linker at the same ratio as with the MACS nickel samples, with the difference that the cross-linking powder was not decorated with the nickel. Similarly to the previous experiments, the etch rate was calculated using the thickness difference, as obtained from the ellipsometer, and the time of the etch process.

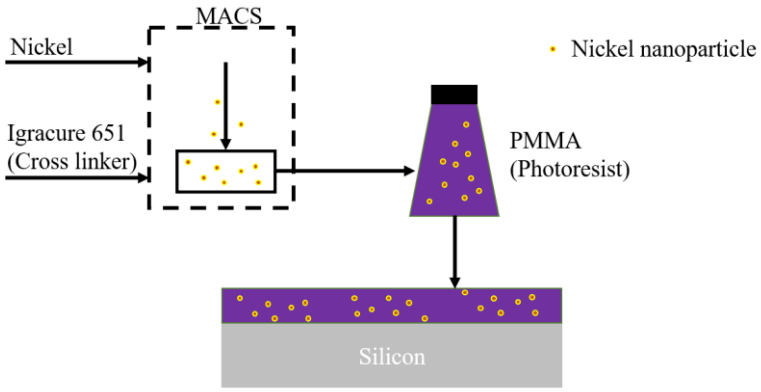

Figure 20: Process flow for the integration of the MACS nanoparticles into PMMA resist. The /cross linker acts as a support powder which can withstand the conditions of the MACS and complete the system. The cross linker enriched with nickel nanoparticles is then mixed with PMMA, after which the formula is spin coated onto the substrate and baked before it is etch tested.

5.1.3 Experimental Results

The proof of principle test experiments were conducted in sequence, with two types of samples being tested; MACS nanocomposite resist and control samples. The results can be seen in Figure 21, which show that on average the MACS nanocomposite resists performed marginally better compared to the control samples, by resulting with a lower etch rate.

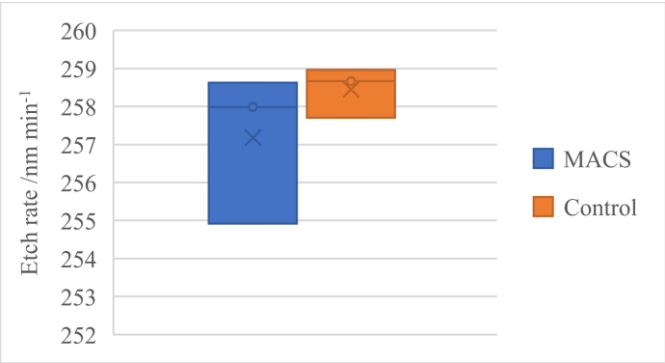

Figure 21: Box and whisker plot of etch rate results of nanocomposite nickel MACS PMMA samples tested in DSi-v, with the xSwan_HighAspectRun9_R05 process. Three samples of each resist were tested in conjunction.

The difference however is very small, and it could fall under the margin of error. However, these preliminary results do show some evidence of the presence and impact of the nickel nanoparticles. The same results have been displayed on Figure 22, where the samples have been displayed in the order that they were tested. Even though a standard inter wafer clean was conducted between each of the samples, there is again evidence that the results were affected by previous runs in the etch tool.

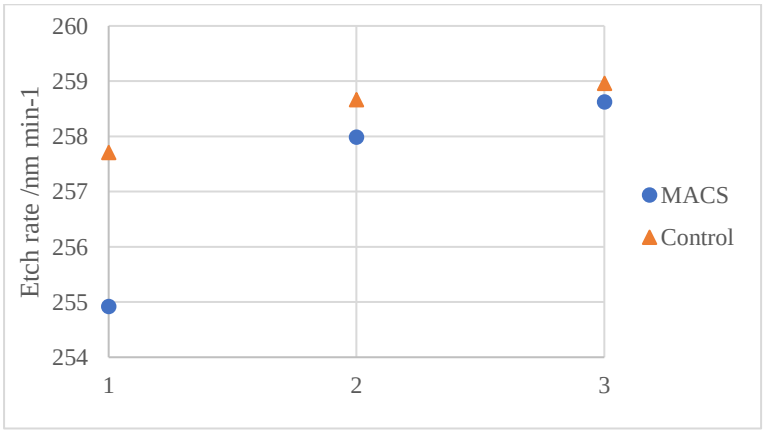

Figure 22: Etch rate results of nanocomposite nickel MACS PMMA samples tested in DSi-v, with the xSwan_HighAspectRun9_R05 process. The scatter graph shows the results in the order that they were tested: the first control sample followed by the first MACS sample, followed by the second control sample, etc.

The results in Figure 22 also suggest an increased efficacy rate of the MACS nanoparticles. This observation is based on the context of the results in sequence 2 and 3, where the results appear more similar. Overall, the improvement rate of the MACS nanoparticles was 1.08% as obtained from the target differences in the etch rates during the first MACS and control resists. However, the average improvement was

only 0.49% when all of the 3 results are taken into account. The average etch rate of all 3 MACS nanoparticle implanted in resist is 257.18 nm/min compared to 258.44 nm/min for the control samples. It is difficult to comment on the results because the specific loading rate of the nickel in the MACS sample remains uncertain. The best that can be claimed at this preliminary stage is that a fabrication scheme has been designed to incorporate MACS clusters, and extensive testing is needed.

5.1.4 Characterisation of the MACS samples by XPS

The XPS analysis struggled to find evidence of nickel nanoparticles in the MACS samples as well as in the conventional nickel powder nanoparticle samples, as shown in the material stoichiometry breakdown on Table 8.

Table 8: XPS Result analysis of the MACS sample of unknown nickel nanoparticle content, and additional 0 mg (control), 15 mg and 25 mg samples. XPS did not see major differences between the samples which would help to establish the nickel concentrations, instead the results being dominated by the photoresist chemistry and etch process by-products shown in the analysis.

Sample Identifier	**Al 2p %**	**C 1s %**	**F 1s %**	**N 1s %**	**Ni 2p %**	**Ni 3p %**	**O 1s %**	**S 2p %**	**Si 2p %**
Control-1-3	0.2	49.8	37.6	0.2	Not observed	Not observed	12.1	0.1	0.0
15mgNi-2-3	0.0	73.8	0.0	0.0	Not observed	Not observed	25.8	0.0	0.4
25mgNi-3-3	0.0	74.2	0.0	0.0	Not observed	Not observed	25.6	0.0	0.2
MACS_Ni-4-3	0.2	49.9	36.9	0.2	Not observed	Not observed	12.4	0.1	0.3

The analysis results were essentially identical for each of the samples. The highest material quantities are carbon and oxygen, which is expected from the photoresist material used. Additionally, sulphur, fluorine and silicon show a weak signal, which arises from the etch process chemistry using O_2 and SF_6 as plasma as well as the silicon substrate material. The aluminium signal likely arose from cross contamination.

The results do not allow for any quantification of Nickel in the photoresist. Interestingly, no Nickel signal was observed even for the higher concentration samples which sets the boundary for detection as higher than that value. The concentration of Nickel could be calculated only from the etch results, but that calculation would not account for a different efficacy rate of the nickel from the MACS compared to the conventionally purchased nanoparticles. One possible reason why the Ni was not detected may be due to oxidisation of nickel during prior handling of the material. An example spectrum from the XPS can be seen in Figure 23.

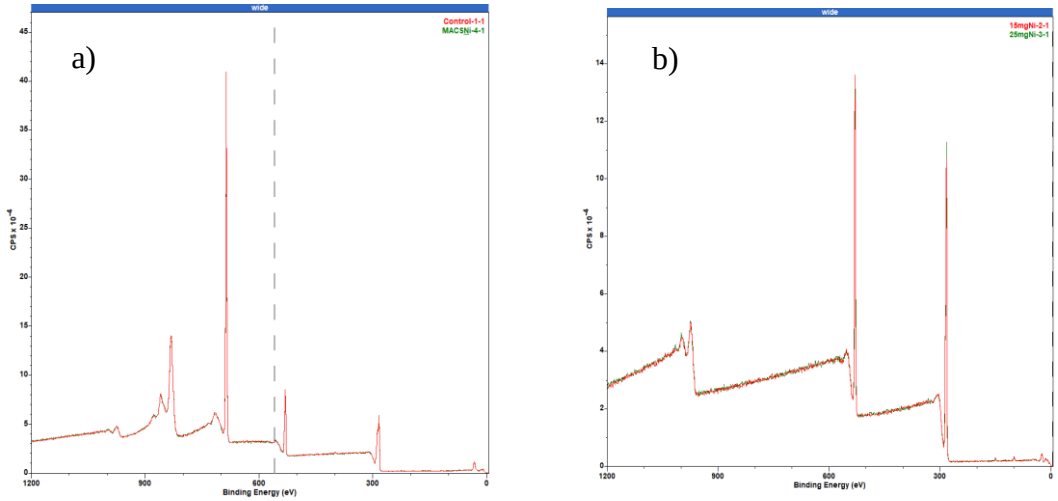

Figure 23: Signals from the XPS which show peaks at different binding energies. The peaks were associated with species that were expected to be present, and other peaks such as Aluminium were identified. a) shows the figure for the control and the MACS samples which were using PMMA, and b) where the 15 and 25 mg samples where the photoresist was MIR-701. Wide scans are shown, however more focused, high-resolution scans were also obtained which showed the same results. The main peaks were expected to be present at 852.6 eV (Ni metal), 853.7 eV (NiO). [37]

5.1.5 Summary

As a basis for future development of nanocomposite resists, a scheme was conceived to implant MACS nanoparticles into PMMA resist by depositing onto a cross linking material, Irgacure 651. The resist material was tested successfully in the DSi-v, with the results showing a marginal improvement in etch resistance between the MACS and the control sample. There was an issue with replicating the etch rates with successive runs, especially for the MACS samples, which is the same effect as shown in the previous experiments with a different resist. This can be seen by the standard deviation of the MACS and control samples, which stand at 1.98 and 0.66 respectively. The average improvement rate of the resist contains MACS implanted nickel

nanoparticles over the control samples was 0.49%, while at the first set of samples tested it reached its highest point of 1.08%. The results also show how the etch rate results can vary when the same loading samples are tested in a sequence. While similar etch rates would be expected, the results showed an increase in the etch rate as the experiment progresses. The XPS analysis did not show signals corresponding to the Nickel content, therefore they could not be used to calculate the nickel concentration in the resist. There was no signal shown for either of the 15 and 25 mg of nickel powder samples, which means that the lower limit for nickel detection lies above the loadings used. This may be because of bonding of the material with the photoresist or due to the presence of the oxide layer around the clusters.

5.2 Conclusions of the Project

The experiments have shown evidence that nickel nanoparticles improve the etch resistance of the resists tested. The main set of experiments, using commercially purchased Ni nanoparticles, showed a clear reduction in the etch rates. Variabilities in the results appeared in repeated experiments with the APS tool Consistent behaviour can be observed in the DSi-v tool. The DSi-v maintains a pattern of increasing etch resistance with the increased loading of nickel in the resist. The biggest improvement can be seen in experiments where the loading rate is the highest, at 20 mg/g (mass of nickel nanoparticles/mass of MIR-701 resist). Here the improvement over the initial control sample reached 17%. Loading this high appeared to maintain the performance of the resist. Even though the resist visibly changed colour before spin coating (to dark black - the higher the loading of the resist, the darker the colour of the resulting resist), the structure appeared uniform and agglomerate free suggesting it would be suitable for patterning.

As for the proof of principle experiments, etch rate results of the nickel implanted nanoparticles produced in the MACS show a small improvement in the etch rates compared to the control samples, with the improvement reaching 1.08% at the highest point, and 0.48% on average from the whole data set from the DSi-v. However, the etch rates were found to change for identical samples, with the etch rates increasing for both the nickel and control samples as the experiment progressed. This mirrors the issues with the experiments that were conducted with the purchased nanoparticles. Considering how low is the improvement in the etch rates in the MACS sample experiments, it is likely that the nickel loading is very low. Indeed, the XPS was not

able to detect nickel in the MACS samples, however it was also un-able to detect nickel in the higher loading samples that were prepared for comparison. As the differences between results and improvements are so small, the error from the ellipsometry measurements could also be important. It is therefore difficult to comment quantitively on the results of the MACS experiments. I hope that others will be able to build on and extend this work in the future.

Perhaps the major achievement of the work is that for each set of experiments, with Ni nanoparticle powder and MACS deposition, a scheme was designed and successfully implemented to create nanocomposite resists.

5.3 Future Work

This project served as a pilot laying a basis for future systematic studies of metal nanoparticles in the semiconductor etching industry. The experiments showed some promising results, which could be explored further by optimising the process conditions. The experiments involving the commercially purchased nanoparticles mixed with MIR-701 resist show clear compatibility and improvement in the etch rate. However, more work should be carried out in order to resolve the apparent decline in resist performance with repeated runs. Testing different etch is important, as was shown between the results of the two etch tools. Because the results in the DSi-v were more repeatable, it suggests that the process could be more compatible with the nanoparticles formulations. Further work would help to establish whether there is a technical issue with the APS, or whether the basic nature of the process is what causes this effect. If the effect is assumed to be caused by material accumulation in the etch chamber, optimising the inter wafer process could help to improve the condition. Testing the etch rates at further increased Ni loadings, as well as the ability to strip the nanocomposite resist is also important.

As well as improving the process conditions when testing the etch resistance of the resist, patterning work is essential to establish whether the resist can produce high resolution features in the substrate. These experiments would expose any homogeneity issues with the nanoparticle distribution throughout the resist. Metal containing resists are known to produce high resolution patterns and low line-edge roughness [35]. Achieving this with the Ni formulation would validate the technology for possible use in the semiconductor industry.

The largest novelty here concerns the nanoparticles produced by the MACS. While a first test was conducted of the etch resistance of nickel implanted PMMA, the specific loading of the resist remains unknown. This prevents atomic structure analysis and great deal more work is needed. Samples of different loading of nickel would establish the relationship between the loading and the etch rate, as with the experiments of commercial nanoparticles. Again, patterning would be crucial for future work.

Bibliography

[1] H. Xu, V. Kosma, E. P. Giannelis and C. K. Ober, “In Pursuit of Moore's Law: polymer chemistry in action,” *Polymer Journal,* pp. 1-11, 2017.

[2] E. D. Martinez, A. Prado, M. Gonzales, S. Anguiano, L. Tosi, L. Salazar Alarcón and H. Pastoriza, “Recent Advances on Nanocomposite Resists With Design Functionality for Lithographic Microfabrication,” *Frontiers in Materials,* 2021.

[3] S. D. Kumar, J. B. Kumar and H. M. Mahesh, “Synthesis of Inorganic Nanomaterials,” in *Synthesis of Inorganic Nanomaterials*, Elsevier, 2018, pp. 59-88.

[4] M. A. Fraga, M. Bosi and M. Negri, “Silicon Carbide in Microsystem Technology - Thin Film Versus Bulk Material,” in *Advanced Silicon Carbide Devices and Processing*, 2015.

[5] J. Y. Tsao, S. Chowdhury, M. A. Hollis, D. Jena, N. M. Johnson, K. A. Jones, R. J. Kaplar, S. Rajan, C. G. Van de Walle, E. Bellotti, C. L. Chua, R. Collazo, M. E. Coltrin, J. A. Cooper, K. R. Evans, S. Graham, T. A. Grotjohn and E. Heller, “Ultrawide-Bandgap Semiconductors: Research Opportunities and Challenges,” *Advanced Electronic Materials,* 2018.

[6] D. Widmann, H. Mader and H. Friedrich, Technology of Integrated Circuits, Springer, 2000.

[7] Z. Tian, X. Chen and X. Xu, “Molecular dynamics simulation of the material removal in the scratching of 4H-SiC and 6H-SiC substrates,” *International Journal of Extreme Manufacturing,* 2020.

[8] J. Kräußlich, W. Matz, A. Bauer, P. Reischauer, N. Schell and K. Goetz, “Structure refinement of the silicon carbide polytypes 4H and 6H:

unambiguous determination of the refinement parameters," *Acta Crystallographica Section A: Foundations of Crystallography,* 2001.

[9] H. Okada, M. Baba, M. Furukawa, K. Yamane, A. Wakahara and H. Sekiguchi, "Formation of SiO2 Film by Chemical Vapour Deposition Enhanced by Atomic Species Extracted from a Surface-wave Generated Plasma," in *The Irago Conference*, 2017.

[10] J. D. Plummer, M. D. Deal and B. P. Griffin, Silicon VLSI Technology, Stanford: Prentice Hall, 2000.

[11] C. Martin, G. Rius, A. Llobera, A. Voigt, G. Gruetzner and F. Perez-Murano, "Electron beam lithography at 10 keV using an epoxy based high resolution negative resist," *Microelectronic Engineering,* vol. 84, pp. 1096-1099, 2007.

[12] C. Luo, C. Xu, L. Lv, H. Li, X. Huang and W. Liu, "Review of recent advances in inorganic photoresists," *RSC Advances,* vol. 10, pp. 8385-8395, 2019.

[13] M. A. McCord and M. J. Rooks, Handbook of Microlithography, Micromachining and Microfabrication, London: SPIE, 1997.

[14] S. A. Maier and H. A. Atwater, "Plasmonics: Localisation and guiding of electromagnetic energy in metal/dielectric structures," *Journal of Applied Physics 98,* 2005.

[15] H. Xu, V. Kosma, E. P. Giannelis and C. K. Ober, "In pursuit of Moore's Law: polymer chemistry in action," *Polymer Journal,* 2017.

[16] R. E. Palmer, R. Cai and J. Vernieres, "Synthesis without solvents: the cluster (nanoparticle) beam route to catalysts and sensors," *Accounts of Chemical Research,* pp. 2296 - 2304, 2018.

[17] M. S. Alfonso, C. Lapeyronie, M. Goubet, B. Viala and J. H. Tortai, "Enhanced dielectric properties of epoxy-based photoresist nanocomposites using carbon-coated nickel nanoparticles for high voltage integrated capacitors," *Composites Science and Technology,* 2021.

[18] Z.-M. Dang, Y.-H. Lin and C.-W. Nan, “Novel Ferroelectric Polymer Composites with High Dielectric Constants,” *Advanced Materials,* 2003.

[19] R. G. Polusen, “Plasma etching in integrated circuit manufacture - A review,” *Journal of Vacuum Science & Technology,* vol. 14, pp. 256-274, 1977.

[20] R. Knizikevicius, “Simulations of Si and SiO2 Etching in SF6+O2 Plasma,” *Acta Physica Polonica A,* vol. 117, no. 3, pp. 478-483, 2010.

[21] K. R. Ryan and I. C. Plumb, “A model for the etching of silicon in SF6/O2 Plasmas,” *Plasma Chemistry and Plasma Processing,* vol. 10, no. 2, pp. 207-229, 1990.

[22] F. Laermer, A. Schilp, K. Funk and M. Offenberg, “Bosch deep silicon etching: improving uniformity and etch rate for advanced MEMS applications,” in *Twelfth IEEE International Conference in Micro Electro Mechanical Systems,* Orlando, 1999.

[23] K. C. Ober, H. Xu, V. Kosma, K. Sakai and E. P. Giannelis, “EUV photolithography: resist progress and challenges,” in *Proceedings of SPIE,* San Jose, 2018.

[24] F. Müller, W. Peukert, R. Polke and F. Stenger, “Dispersing nanoparticles in liquids,” *International Journal of Mineral Processing,* pp. S31-S41, 2004.

[25] M. S. Alfonso, C. Lapeyronie, M. Goublet, B. Viala and J. H. Tortai, “Enhanced dielectric properties of epoxy-based photoresist nanocomposites using carbon-coated nickel nanoparticles for high-voltage integrated capacitors,” *Composites Science and Technology,* 2021.

[26] A. Ghamartale, S. Afzali, N. Rezaei and S. Zendehboudi, “Asphaltene Deposition Control by Chemical Inhibitors,” in *Polymeric Nanomaterials in Nanotheraupetics,* Amsterdam, Elsevier, 2019.

[27] E. S. Lambers, C. N. Dykstal, J. M. Seo, J. E. Rowe and P. H. Holloway, “Room-temperature oxidations of Ni(110) at low and atmospheric oxygen pressures,” *Oxidation of Metals,* vol. 45, pp. 301-321, 1996.

[28] J. N. Hilfiker, R. Dammel, C. L. Henderson and R. A. Synowicki, “Refractive-index measurements of photoresist and antireflective coatings ith variable angle spectroscopic ellipsometry,” *Proceedings of SPIE - The International Society for Optical Engineering,* 1998.

[29] D. E. Aspnes, “Spectroscopic ellipsometry - Past, present, and future,” *Thin Solid Films,* vol. 571, pp. 334-344, 2014.

[30] d. Ricardo, “Plasma etching of Si and SiO2 in SF6-O2 mixtures,” *Journal of Applied Physics,* vol. 52, 1981.

[31] J. Xu, S. Murphy, D. Xiong, R. Cai, X.-K. Wei, M. Heggen, E. Barborini, S. Vianti, R. E. Dunin-Borkowski, R. E. Palmer and L. Liu, “Cluster beam deposition of ultrafine cobalt and ruthenium clusters for efficient and stable oxygen evolution reaction,” *ACS Applied Energy Materials,* pp. 3013-3018, 2018.

[32] R. Cai, F. Martelli, J. Vernieres, S. Albonetti, N. Dimitratos, C. Tizaoui and R. E. Palmer, “Scale-up of cluster beam deposition to the gram scale with the matrix assembly cluster soirce for heterogeneous catalysis (catalytic ozonation of nitrophenol in aqueous solution),” *ACS Applied Materials & Interfaces,* pp. 24877-24882, 2020.

[33] D. J. Carbaugh, J. T. Wright and F. Rahman, “Negative tone photolithography with photo-sensitised polymethyl methacrylate (PMMA),” *Microelectronic Engineering,* vol. 171, pp. 53-59, 2017.

[34] F. Rahman, D. J. Carbaugh, J. T. Wright, P. Rajan and S. G. Pandya, “A review of polymethyl methacruylate (PMMA) as a versatile lithographic resist - With emphasis on UV exposure,” *Microelectronic Engineering,* vol. 224, 2020.

[35] M. S. M. Saifullah, N. Tiwale and R. Ganesan, “Review of metal-containing resists in electron beam lithography: perspectives for ultravioled patterning,” *Journal of Micro/Nanolithography, MEMS, and MOEMS,* vol. 21, 2022.

[36] J. Pudlauskaitė, I. Prosyčevas, V. Jankauskaitė and T. Kleveckas, “Photoresist modification by silver colloid solution: the role of silver nanoparticle content,” *Proceedings of the Estonian Academy of Sciences,* 2012.

[37] F. Aydinoglu, A. Pan, C. Zhu and B. Cui, “Effect of oxygen plasma cleaning on nonswitching pseudo-Bosch etchong of high aspect ratio silicon pillars,” *Journal of Vacuum Science & Technology,* vol. 38, 2020.

[38] H. W. Nesbitt, D. Legrand and G. M. Bancroft, “Interpretation of Ni2p XPS spectra of Ni conductors and Ni insulators,” *Phys Chem Minerals,* pp. 357-366, 2000.